Received: 15 January 2021 | Revised: 19 April 2021 | Accepted: 24 April 2021

DOI: 10.1111/jace.17891

Journal of the American Ceramic Society

ORIGINAL ARTICLE

Thermally stimulated depolarization current measurements on degraded lead zirconate titanate films

Betul Akkopru-Akgun[1,2] | **Daniel M. Marincel**[3] | **Kosuke Tsuji**[3] | **Thorsten J. M. Bayer**[3] | **Clive A. Randall**[3] | **Michael T. Lanagan**[1,4] | **Susan Trolier-McKinstry**[1,2]

[1]Center for Dielectrics and Piezoelectrics, Materials Research Institute, The Pennsylvania State University, University Park, Pennsylvania, USA

[2]Department of Materials Science and Engineering, The Pennsylvania State University, University Park, Pennsylvania, USA

[3]Department of Physics and Optical Engineering, Rose-Hulman Institute of Technology, Terre Haute, Indiana, USA

[4]Department of Engineering Science and Mechanics, The Pennsylvania State University, University Park, Pennsylvania, USA

Correspondence
Betul Akkopru-Akgun, Center for Dielectrics and Piezoelectrics, Materials Research Institute, The Pennsylvania State University, University Park, Pennsylvania 16802, USA.
Email: betul.akkopru@gmail.com

Funding information
The National Science Foundation, as part of the Center for Dielectrics and Piezoelectrics, Grant/Award Number: IIP-1841453 and IIP-1841466

Abstract

Charge transport mechanisms governing DC resistance degradation in ferroelectric films are influenced by defects, particularly oxygen vacancies. This paper demonstrates that oxygen vacancies migrate in lead zirconate titanate (PZT) films under a DC bias field and contribute to resistance degradation. Model PZT thin films were developed in which the concentration and distribution of oxygen vacancies were controlled via (a) changing the dopant type and concentration from 1%–4% Mn (acceptor) to 1%–4% Nb (donor) or (b) annealing undoped PZT films at varying partial pressures of PbO. The presence of associated (immobile) and dissociated (mobile) oxygen vacancies was distinguished by thermally stimulated depolarization current (TSDC) measurements. The impact of mobile oxygen vacancies on local defect chemistry and associated charge transport mechanisms was explored by electron energy loss spectroscopy (EELS). For Mn-doped PZT films, following resistance degradation, TSDC studies revealed only one depolarization peak with an activation energy of 0.6–0.8 eV; this peak was associated with ionic space charge presumably due to migration of oxygen vacancies. The magnitude of the depolarization current peak increased with increasing degradation times. A similar depolarization current peak attributed to the existence of mobile oxygen vacancies was also observed for undoped and Nb-doped PZT films; the magnitude of this peak decreased as the Nb or PbO contents in PZT films increased. An additional TSDC peak associated with polaron hopping between Ti^{3+} and Ti^{4+} was found in both Nb-doped PZT films and undoped PZT films annealed under low PbO partial pressure. Degraded Nb-doped samples exhibited a chemical shift in the $TiL_{2,3}$ peak to lower energy losses and the appearance of shoulders on the t_{2g} and e_g peaks, implying a reduction of Ti cations in regions near the cathode.

KEYWORDS

defect states, EELS, electrical conductivity, ferroelectricity/ferroelectric materials, lead zirconate titanate, PZT thin films, resistance degradation, thermally stimulated depolarization current, thin films

1 | INTRODUCTION

Over the last few decades, ferroelectric thin films have been utilized in a variety of microelectromechanical (MEMS) devices, including adjustable optics,[1] ink jet printers,[2] ultrasound transducers,[3] resonators,[4] and energy harvesters.[5] MEMS are often driven at significantly higher electric fields than bulk piezoelectrics; therefore, it is important to develop ferroelectric thin films which can operate under high electric fields. However, the use of high field operation imposes strict constraints on the DC resistance degradation in order to achieve reliable ferroelectric thin films with long lifetimes.

DC resistance degradation has been comprehensively studied in alkaline-earth titanate perovskites such as acceptor-doped $SrTiO_3$ and $BaTiO_3$. It is generally recognized that electromigration of oxygen vacancies under a DC bias field toward the cathodic region underpins electrical degradation in these materials. In $SrTiO_3$ and $BaTiO_3$, the primary source of both oxygen vacancies and holes is acceptor ions. To maintain electroneutrality, the concentration of electrons increases in the cathodic region during degradation, whereas the hole concentration rises in the oxygen vacancy-depleted anodic region. As a result, the anodic region becomes a hole conductor, whereas in the cathodic region electron conductivity is dominant; in the titanates, the excess electrons can be trapped by Ti^{4+} to form Ti^{3+}.[6]

A comprehensive study on the evolution of defect distributions of lead zirconate titanate (PZT) materials is needed. For PZT films, the high PbO volatility during crystallization leads to the formation of oxygen vacancies and holes.[6,7] The defect chemistry becomes more complicated by the hybridization of the lone electron pair in Pb^{2+} and also by the variation in oxidation states upon thermal treatment.[8] For example, the Pb^{2+} site can act as a shallow hole trap (to form Pb^{3+}). A greater knowledge of the behavior of mobile point defects is essential to better understand DC resistance degradation in PZT thin films. In reality, experiments that can probe point defects in thin films are not practical and only a few studies link the dominant charge transport mechanisms to the defect chemistry of PZT films.[6-14]

In this work, thermally stimulated depolarization current measurements (TSDC) were employed to probe the defects that lead to electrical degradation in PZT films. The nature and concentration of defects such as dipoles, trap charges, and mobile ions, can be determined via TSDC analysis. The activation energies and the concentration of those defects can also be estimated using TSDC.[15-17]

TSDC analysis of ferroelectrics is complicated by the existence of background currents arising from the pyroelectric effect.[18] Nonetheless, Wu and Sayer were able to explore the link between aging and the TSDC peak associated with oxygen vacancies in piezoelectric thin films by minimizing pyroelectric contributions to the signal.[18] Okino et al. used thermally stimulated current, reporting that polarization fatigue was caused by domain pinning from trapped charges. However, the physical origin of the trapped charges was not identified.[19]

The main objective of this study was to explore the changes in defect concentrations and defect distributions upon electrical degradation in undoped, donor (Nb), and acceptor (Mn) doped PZT films using TSDC. In particular, the manner in which defect type and concentration affect the electrical conduction and degradation phenomena in PZT films was investigated. The origins of dielectric relaxations in undoped, Mn, and Nb-doped PZT films were explored and linked to the time-dependent leakage current associated with oxygen vacancy migration upon degradation. The migration of oxygen vacancies under a DC bias is discussed and related to charge transport mechanisms in PZT films. Additionally, the electron polaron hopping between Ti^{3+} and Ti^{4+} was proven by complementary findings of TSDC and electron energy loss spectroscopy (EELS) analyses.

2 | EXPERIMENTAL PLAN

2.1 | Preparation of undoped, Mn, and Nb-doped PZT thin films by sol-gel method

Undoped, acceptor-doped (Mn), and donor-doped (Nb) PZT thin films with dopant concentrations varying from 0.5 to 4 mol% were grown on $Pt/Ti/SiO_2/Si$ substrates (Nova Electronic Materials, Flower Mound, TX) by chemical solution deposition. The preparation of solutions is similar to that described elsewhere.[20,21] The final film compositions of: $PbZr_{0.52(1-x)}Ti_{0.48(1-x)}Mn_xO_{3-\delta}$, where $x = 0.005$–0.040 and $Pb_{(1-0.5x)}Zr_{0.52(1-x)}Ti_{0.48(1-x)}Nb_xO_3$, where $x = 0.005$–0.040, were calculated presuming B site occupancy of Mn and Nb ions.

For film growth, PZT solution was spin-coated on platinized silicon substrates at 1500 rpm for 30 s. Then, each PZT layer was pyrolyzed at 250°C and 450°C for 3 min, respectively. Following pyrolysis treatment, the PZT film crystallized at 700°C for 60 s via rapid thermal annealing under flowing O_2. This process was repeated till a film thickness of 400 nm was achieved. To remove surface pyrochlore, a PbO layer was spun onto the PZT film, followed by annealing at 700°C in air. Finally, the sample was immersed in a 4 M acetic acid solution for 60 s to eliminate residual PbO on the surface of the PZT film.

Following crystallization, undoped PZT films were exposed to a second annealing treatment at 670°C under varying PbO partial pressures for 1 h. In this study, the partial pressure of the PbO precursor, tetraethyl lead, was varied between 3.53×10^{-5} Torr and 2.85×10^{-4} Torr in order to control the PbO nonstoichiometry.[22]

3 | MATERIALS CHARACTERIZATION

Characterization techniques used to explore the structural and electrical properties of PZT films are described elsewhere.[23] Specifically, grazing incidence X-ray diffraction (GIXRD) and field-effect scanning electron microscopy (FESEM) were used to analyze the structure of the undoped samples after annealing in a PbO environment.

3.1 | TSDC measurements of PZT films

TSDC differentiates relaxation currents originating from trapped charges, space charge, and defect dipoles based on their relaxation kinetics. The test conditions for the TSDC measurements in this work are shown in Figure 1A. PZT thin films were wire bonded to two Pt pieces to facilitate electrical contacts. First, the sample was heated to the degradation temperature (T_p) of 180°C and then electrically degraded under DC field to orient or move defects. After degrading the sample for 12 h under an electric field ranging from 250 to 400 kV/cm, the sample was cooled to room temperature (T_0) with a cooling rate of 10 K/min where the defect dipoles, space charges, and trapped charges were frozen into the degraded state. Subsequently, the sample was shorted and the electric field removed. Then, the sample was heated at a constant rate of 4, 6, 8, or 10°C/min and the relaxation current from the depolarization of relaxing defects was recorded at temperatures ranging from 25°C to 300°C with a HP 4140b pA meter. Electrical connections from the sample to pA meter were achieved by using BNC and triaxial cables in order to minimize the leakage current arising from the cable itself. The effect of the electric field, heating rate, dopant type and concentration, and the annealing atmosphere on the depolarization current, and associated trapped charges was investigated.

TSDC can be mathematically described for a single relaxation using the equation[24]

$$J(T) = n_0 s \exp\left(\frac{-E_a}{k_b T}\right) \cdot \exp\left[-s/\beta \int_{T_0}^{T} \left(\frac{-E_a}{k_b T^I}\right) dT^I\right] \quad (1)$$

$$s = \beta \frac{E_a}{k_b T_{max}^2 \exp\left(\frac{-E_a}{kT_{max}}\right)}$$

where E_a is the activation energy, T_{max} is the temperature corresponding to the peak maximum, β is the heating rate, n_0 is the concentration of dipoles, and s is a geometrical factor relying on the dipole orientation. It is well known that the position and shape of TSDC peaks are affected by the heating rate. The TSDC peak becomes narrower and is shifted to higher temperatures as the heating rate increases. High heating rates enhance the dipolar interaction process upon relaxation, leading to higher depolarization currents.[25] The concentration of dipoles, n_0, can also be calculated from Equation 1.

Before analyzing each peak to derive the activation energy and concentration of defects, the magnitude of the TSDC signal arising from depolarization of the ferroelectric polarization was investigated by assessing the piezoelectric response via double beam laser interferometer (DBLI). An equivalent sample was heated to a temperature just below 200°C, where the first TSDC peak emerged. It was found that for temperatures up to T_1, the piezoelectric $d_{33,f}$ coefficient recovered its original value on cooling to room temperature (Figure 1B). Therefore, up to this temperature reorientation of the ferroelectric polarization is not expected to contribute to the measured TSDC signal in this temperature range.

4 | RESULTS AND DISCUSSION

4.1 | Structural properties of PZT films

The surface morphology and structure of PZT films after annealing at 670°C under different PbO partial pressures were studied by GIXRD and FESEM. The GIXRD studies (Figure 2) reveal that undoped PZT films are approximately randomly oriented and have a perovskite structure. No secondary phases such as excess PbO or pyrochlore were found in the XRD results. Moreover, the intensity and positions of XRD peaks are the same for all PbO contents, indicating that the crystallinity was governed by the initial crystallization step.

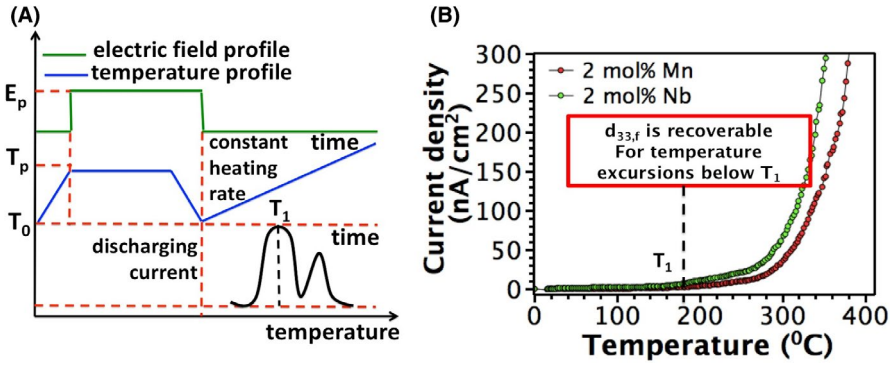

FIGURE 1 (A) TSDC measurement process and (B) The current response to increasing temperature in 2 mol% Mn and 2 mol% Nb-doped PZT films [Color figure can be viewed at wileyonlinelibrary.com]

Figure 3 shows the FESEM micrographs of undoped PZT films annealed at different PbO activities. As shown in Figure 3, the deposited PZT films were smooth and homogeneous; no crack formation was observed. SEM results confirmed that grain size for undoped PZT films with different PbO contents is similar and varies between 30–150 nm. This indicates that grain size remains relatively constant while annealing in a PbO-rich atmosphere. As was the case for the undoped PZT films, no secondary phases, such as PbO or pyrochlore were observed for Mn or Nb-doped PZT films.[21] The deposited PZT films were smooth, homogenous, and crack free. The grain size in both Mn- and Nb-doped PZT films is similar and ranges from 40 to 160 nm. The details of structural characterization results of Mn- and Nb-doped PZT films can be found elsewhere.[21]

4.2 | Thermally stimulated depolarization current measurement results

TSDC measurements were carried out on degraded Nb- and Mn-doped and undoped PZT films annealed under varying PbO partial pressures to probe electronic and ionic defects resulting in electrical degradation. Figure 4 shows the TSDC spectra obtained from degraded Mn- and Nb-doped PZT films that were polarized under electrical fields ranging from E_p = 200 to 400 kV/cm at T_p = 180°C for 12 h, measured with a heating rate of β = 8°C/min. The continuous increase in the background current above 300°C in Figure 4 arises from the pyroelectric effect.

The physical origin of the thermally stimulated current was explored by studying the dependence of T_{max} (Figure 4) on the electric field. For a constant heating rate, the temperature of the current peak shifts in a well-defined manner with increasing electric field; T_{max} can (a) shift to lower temperatures when the relaxation current is associated with trapped charges, (b) shift to higher temperatures when the physical origin of TSDC current is space charge, and (c) remain fixed when the TSDC current arises from defect dipoles.[26-29] As shown in Figure 4A, the TSDC data for Mn-doped PZT films show a single peak, with T_{max} from 204°C to 220°C, for different electric fields. It is readily seen in Figure 4A that T_{max} shifted to higher temperatures with increasing electrical fields, suggesting that the origin of the TSDC depolarization

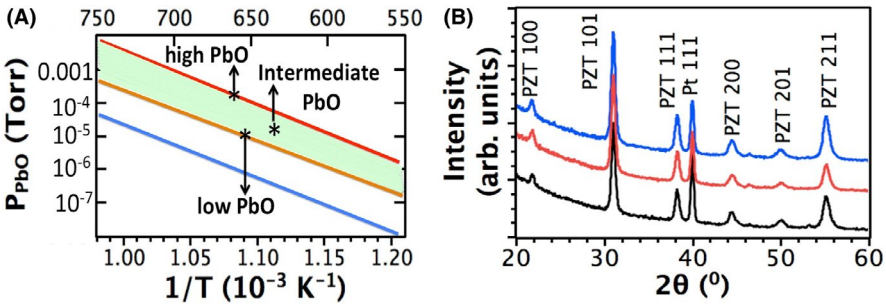

FIGURE 2 The phase stability diagram of PbO, $PbTiO_3$, and $PbZrO_3$ at distinct temperatures. The red, orange, and blue lines denote the required equilibrium PbO partial pressure for PbO (g) → PbO (s), $PbZrO_3$ → PbO (g) + ZrO_2, and $PbTiO_3$ → PbO (g) + TiO_2, respectively. The shaded region represents the required range for PZT perovskite equilibrium,[22,40] (B) XRD diffraction patterns of approximately randomly oriented PZT films indicating phase pure perovskite for (A) low, medium, and high PbO partial pressure [Color figure can be viewed at wileyonlinelibrary.com]

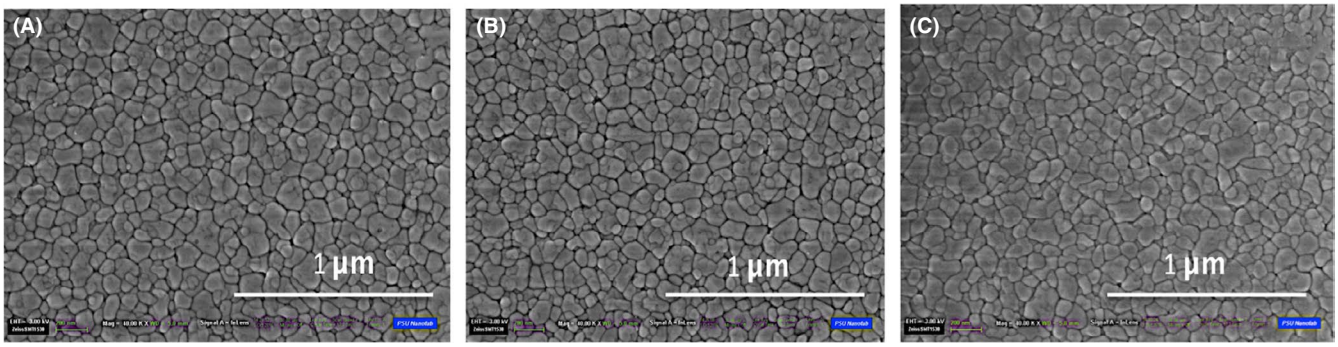

FIGURE 3 Top surface SEM images of PZT films annealed at distinct PbO partial pressures: (A) low PbO partial pressure (yellow line in Figure 2),(B) intermediate PbO partial pressure, and (C) high PbO partial pressure (red line in Figure 2). FESEM images were taken after patterning of Pt top electrodes [Color figure can be viewed at wileyonlinelibrary.com]

peak is associated with a space charge, probably due to the migration of oxygen vacancies. This, coupled with the fact that the magnitude of this peak increases with Mn concentration, demonstrates that this peak is also not due to reorientation of the ferroelectric polarization.

Three distinct methods were used to determine the activation of the TSDC peak. In the first approach, the initial rise model, the first exponential term of Equation (1) controls the temperature rise of the initial current. Thus, ln J_D versus $1/T$, gives rise to a straight line, and the activation energy was estimated from the slope of this line as 0.65 ± 0.04 eV (Figure 5A). In the second method, the FWHM of TSDC peak was used to determine the activation energy (Figure 5B) via Equation 2:

$$E_a = 2.30 k_b T^2_{max} / \Delta T_{1/2} \quad (2)$$

where T_{max} is the temperature corresponding to the peak maximum, $\Delta T_{1/2}$ is the FWHM of TSDC peak. It should be noted that all the expressions in Equation 2 relate to a single Debye process where E_a has a unique value. An activation energy of 0.73 ± 0.03 eV was found.

In the third technique, the heating rate dependence of the TSDC peak position was used to estimate the activation energy of the TSDC relaxation current. The peak position, $T = T_{max}$, is related to the heating rate β through an Arrhenius equation.[30]

$$\ln\beta = \frac{-E_a}{k_b}\left(\frac{1}{T_{max}}\right) + \text{const} \quad (3)$$

$$\ln\left(\frac{T^2_{max}}{\beta}\right) = \frac{E_a}{k_b T_{max}} + \ln\left(\frac{\tau_0 E_a}{k_b}\right) \quad (4)$$

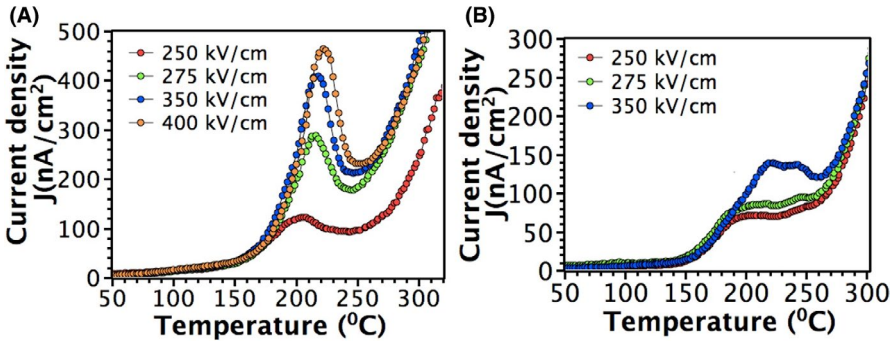

FIGURE 4 Evolution of TSDC peaks with increasing electrical field in (A) 2 mol% Mn, (B) 2 mol% Nb-doped PZT films using a ramp rate of 8°C/min. Samples were poled under a dc bias of 250–400 kV/cm at a temperature of 180°C for 12 h [Color figure can be viewed at wileyonlinelibrary.com]

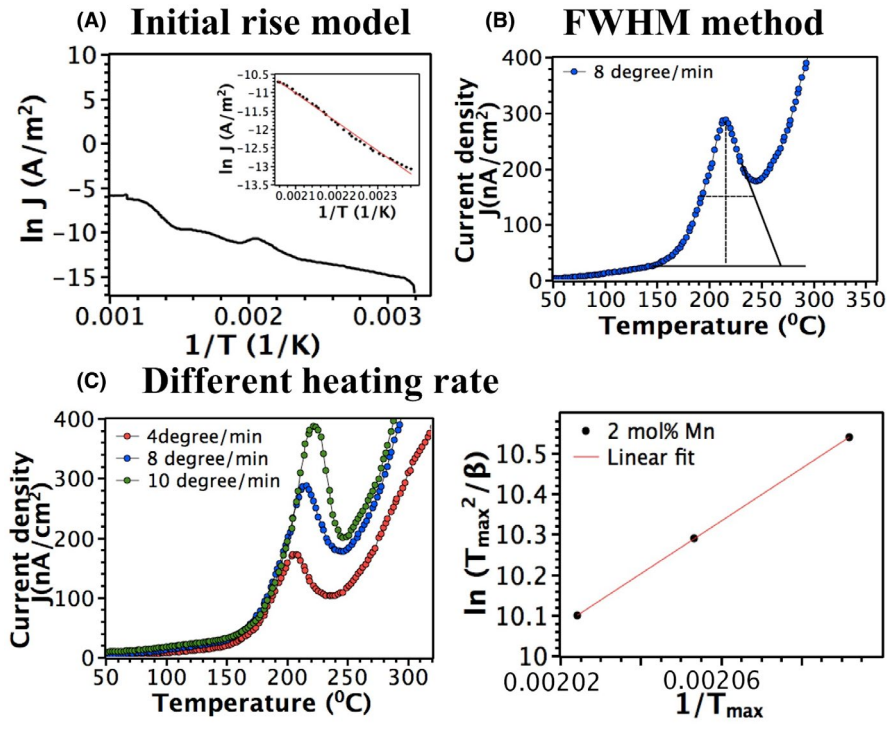

FIGURE 5 Estimation of activation energies for TSDC peaks arising from 2 mol% Mn-doped PZT films using three distinct methods: (A) initial rise model, (B) FWHM method, and (C) different heating rate (6–10°C/min). The films were degraded under an electric field of 275 kV/cm at 180°C for 12 h [Color figure can be viewed at wileyonlinelibrary.com]

here k_b is Boltzmann's constant, τ_0 is the characteristic relaxation time, and E_a is the activation energy associated with the TSDC peak. An activation energy of 0.58 ± 0.02 eV was derived from the plot of $\ln\left(\frac{T^2_{max}}{\beta}\right)$ as a function of $1/T_{max}$ (Figure 5C). The activation energies estimated from three distinct techniques range from 0.58 to 0.73 eV. It is believed that the activation energy estimated using the heating rate method is more accurate since the heating rate dependence of peak temperature solely depends on relaxation kinetics of tapped charges, defect dipoles, or ionic space rather than background current arising from the pyroelectric effect. The estimated activation energies from all three methods are in good agreement with that for the migration of oxygen vacancies as studied by Wang and colleagues. (0.58 eV).[10]

In contrast to Mn-doped PZT films, TSDC results of degraded Nb-doped PZT films indicate two distinct relaxation current peaks with maxima around 220°C and 280°C (Figure 6). The electric field dependence of the TSDC peaks in Nb-doped PZT films is remarkably different: T_{max} of the low-temperature peak shifts to higher temperature with increasing electric field, which is characteristic of space charge polarization. The position of the high-temperature peak shifts slightly to lower temperatures with increasing electric field. A linear relation was found between the peak temperature T_{max} and the square root of the applied field, $E^{1/2}$, indicating relaxation of trapped charges. By using the heating rate method, the activation energies of low- and high-temperature peaks were estimated to be 0.61 ± 0.06 and 0.18 ± 0.05 eV, respectively. These values are similar to those previously reported for the diffusion of mobile oxygen vacancies and electron hopping between Ti^{3+} and Ti^{4+} in the perovskite structure, respectively.[15,16] No significant variation in the amplitude of TSDC peaks for different heating rates (4–8°/min) was observed in Nb-doped PZT films. This might be related to the increased contribution of pyroelectric current to the depolarization current at temperatures higher than 200°C–220°C. (Figure 1)

TSDC was also carried out on undoped PZT films annealed at varying PbO pressures, where the only source of oxygen vacancy formation is the possibility of PbO loss either to the bottom electrode or to the atmosphere during the high-temperature crystallization steps. The PbO partial Schottky defect concentration of films in the undoped PZT films was adjusted using the PbO control furnace, where the lead oxide partial pressure is controlled using a tetraethyl lead source. Figure 7 indicates TSDC data for undoped PZT films with low, medium, and high PbO contents. The magnitude of the TSDC peak attributed to the relaxation of mobile oxygen vacancies diminishes gradually with increasing PbO content in PZT films, indicating that the oxygen vacancy concentration is lowest for films with the highest lead content. It is expected that annealing PZT films at high PbO activities minimizes PbO evaporation and therefore decreases the partial Schottky defect concentration in PZT films when lead vacancies are compensated by oxygen vacancies and holes (Equation 5).[11-14,31,32]

Moreover, the high-temperature TSDC peak at 280°C, attributed to electron hopping between Ti^{4+} and Ti^{3+} sites, was only observed in PZT films with low PbO contents. It is believed that a high concentration of oxygen vacancies accumulates near the cathode of PZT films with low PbO contents during electrical degradation. These vacancies are charge compensated by electrons trapped on Ti sites. It is possible that the inability to detect this signal in undoped PZT films

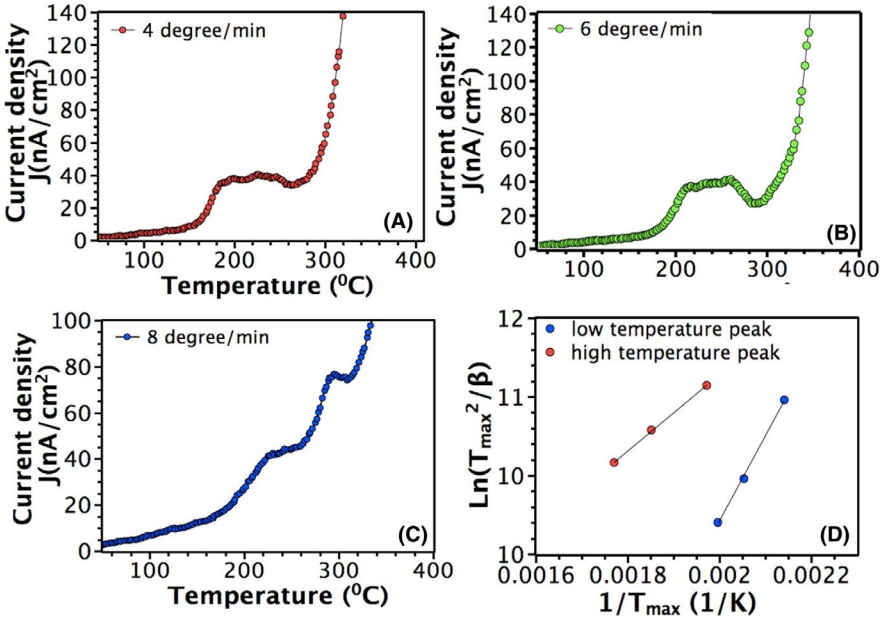

FIGURE 6 (A–C)Thermally stimulated depolarization current data of 2% Nb-doped PZT films for different heating rates (4 and 8°/min), (D) Estimation of activation energies for the low- and high-temperature TSDC peaks using heating rate method. The films were degraded at 180°C under an electric field of 350 kV/cm for 12 h [Color figure can be viewed at wileyonlinelibrary.com]

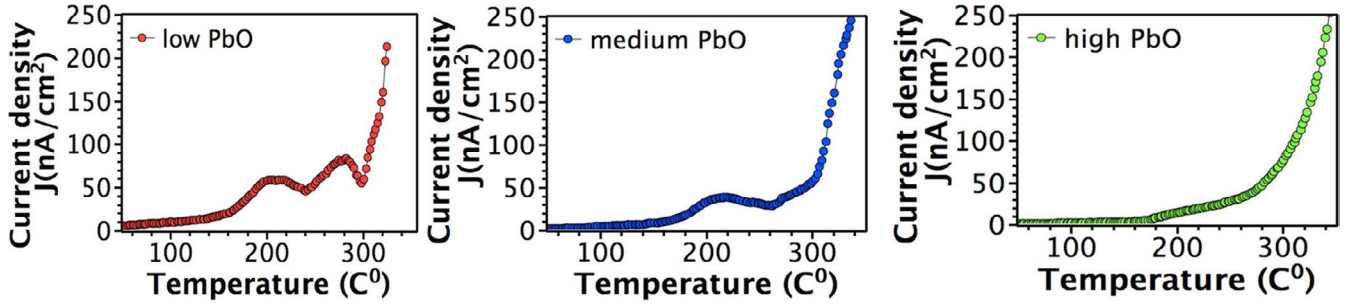

FIGURE 7 TSDC spectra in PZT films annealed under low, medium, and high PbO activities. TSDC data were attained after degrading the films under an electric field of 275 kV/cm at 180°C for 12 h. A 6°/min heating rate was used to attain TSDC peaks [Color figure can be viewed at wileyonlinelibrary.com]

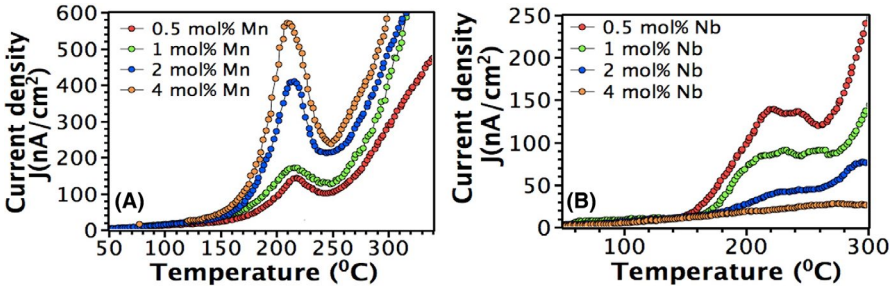

FIGURE 8 Evolution of TSDC peaks in degraded PZT films with increasing (A) acceptor (Mn) dopant concentration, and (B) donor (Nb) dopant concentration. The films were degraded at 180°C under an electric field of 350 kV/cm for 12 h. TSDC data were obtained using a ramp rate of 8°C/min [Color figure can be viewed at wileyonlinelibrary.com]

with high PbO contents was due to a low concentration of oxygen vacancies, and hence a reduction in both the number of trapped electrons and the probability of electron hopping between Ti^{3+} and Ti^{4+}.

$$Pb_{Pb}^{X} + O_{O}^{X} \rightarrow V_{Pb}'' + V_{O}^{\bullet\bullet} + PbO(g) \quad (5)$$

$$2[V_{Pb}''] + [e'] = 2[V_{O}^{\bullet\bullet}] + [h^{\bullet}] \quad (6)$$

After identifying relaxation current peaks for undoped and doped PZT films, the TSDC peak associated with relaxation of mobile oxygen vacancies was further studied in Mn−doped and Nb−doped PZT films as a function of dopant concentration, as presented in Figure 8. The total amount of charge that relaxes due to diffusion of ions can be expressed as[15]:

$$Q_{TSDC} \approx 2avNqt_p \exp\left(-\frac{H}{k_b T}\right) \sinh\left(\frac{qaE_p}{2k_b T_p}\right) = Q_0 \sinh\left(\frac{qaE_p}{2k_b T_p}\right) \quad (7)$$

where N is the density of diffusing ions, ν is ion jump frequency, k is the Boltzmann constant, q is the ionic charge, a is the ionic hopping distance between potential wells of depth H, T_p, E_p, and t_p are the degradation temperature, electric field, and time, respectively.

The concentration of oxygen vacancies that undergo long-range migration during degradation at 180°C under an electric field of 350 kV/cm for 12 h was calculated by integrating the depolarization current peaks (Table 1). The magnitude of the depolarization current peak increases with increasing Mn concentration, suggesting that (a) any defect dipoles that might be present, such as $(Mn_{Ti}'' - V_O^{\bullet\bullet})^X$ and/or $(Mn_{Ti}' - V_O^{\bullet\bullet})'$, dissociate during electrical degradation, and (b) the concentration of mobile oxygen vacancies that give rise to the ionic space charge peak increases with increasing Mn concentration. When Mn is incorporated into PZT, it occupies the B site (Ti or Zr) of the perovskite lattice and is ionically compensated by oxygen vacancies. Thus, an increase in the magnitude of ionic space charge peak with increasing acceptor ion concentration is reasonable.

In contrast, the concentration of mobile oxygen vacancies decreases with increasing Nb concentration (Table 1). This trend is reasonable, as Nb is a donor (Equation 8). The source of the remaining mobile oxygen vacancies in Nb-doped PZT films is likely to be the loss of the PbO during high-temperature treatment. This creates lead and oxygen vacancy partial Schottky defect pairs.

TABLE 1 The concentration of polarized oxygen vacancies, T_{max}, relaxation time, and diffusion coefficient of TSDC results in Nb- and Mn-doped PZT films

	N (cm^{-3})	T_{max} (K)	τ_0 (10^{-4} s)	D_v (cm^2/s)
0.5% Nb	$2.1 \pm 0.1 \times 10^{19}$	498	8.1 ± 0.1	$8.8 \pm 0.1 \times 10^{-15}$
1% Nb	$1.1 \pm 0.1 \times 10^{19}$	502	8.3 ± 0.1	$8.6 \pm 0.1 \times 10^{-15}$
2% Nb	$4.8 \pm 0.1 \times 10^{18}$	507	8.6 ± 0.1	$8.5 \pm 0.1 \times 10^{-15}$
4% Nb	$1.5 \pm 0.1 \times 10^{18}$	514	9.5 ± 0.1	$8.2 \pm 0.1 \times 10^{-15}$
0.5% Mn	$3.1 \pm 0.1 \times 10^{19}$	491	4.9 ± 0.1	$9 \pm 0.1 \times 10^{-15}$
1% Mn	$5.8 \pm 0.1 \times 10^{19}$	488	4.5 ± 0.1	$9.1 \pm 0.1 \times 10^{-15}$
2% Mn	$1.4 \pm 0.1 \times 10^{20}$	486	4.2 ± 0.1	$9.2 \pm 0.1 \times 10^{-15}$
4% Mn	$2.7 \pm 0.1 \times 10^{20}$	483	3.8 ± 0.1	$9.3 \pm 0.1 \times 10^{-15}$

$$2[V_O^{\bullet\bullet}] + [Nb_{Ti}^{\bullet}] + [h^{\bullet}] = 2[V_{Pb}''] + [e'] \quad (8)$$

The maximum temperature, T_{max}, of the TSDC peaks for relaxation of mobile oxygen vacancies is higher for Nb−doped PZT films than their Mn−doped counterparts (Figure 8). T_{max} is closely related to the characteristic relaxation time for polarized species and can be described as[33]:

$$T_{max} = \left[\frac{E_a}{k_b}\beta\tau_0 \exp\left(\frac{E_a}{k_b T_{max}}\right)\right]^{\frac{1}{2}} \quad (9)$$

where E_a is the activation energy, β is heating rate, k_b is Boltzmann's constant, and T_{max} is the relaxation peak temperature. As can be seen in Table 1, the characteristic time, τ_0, for relaxation of the migrated oxygen vacancies decreases with increasing Mn concentration or decreasing Nb concentration. Long-range migration of oxygen vacancies upon electrical degradation results in depletion of oxygen vacancies in the anodic region and accumulation of oxygen vacancies in the cathodic region. When the average oxygen vacancy concentration is high, as in Mn-doped PZT films, even a small degree of electrical degradation results in a measurable depolarization current density; high oxygen vacancy concentrations are correlated with shorter relaxation times. In Nb-doped PZT films with lower oxygen vacancy concentrations, however, stronger degradation conditions are required to achieve the same magnitude of depolarization current density. The diffusion coefficient for long-range migration of oxygen vacancies was calculated using the Nernst–Einstein equation assuming that the velocity is given by L/τ, where L is the film thickness and τ is time that is required for oxygen vacancy migration across the sample thickness of L.

$$D_V = \frac{kT}{2e}u_V = \frac{k_b TL}{2e\tau E}, \quad u_V = \frac{v}{E} \quad (10)$$

where k_b is Boltzmann's constant, ν and u_V are the velocity and the mobility of mobile ions, e is the elementary charge, T is the temperature, and E is the electric field. The estimated diffusion coefficients for oxygen vacancies in Nb- and Mn-doped PZT films shown in Table 1 are in the range of 8–9 × 10^{-15} cm^2/s. This is two orders of magnitude smaller than the reported bulk diffusion coefficient value of 10^{-13} cm^2/s for oxygen vacancy migration in PZT ceramics at 580°C.[10] Based on the assumption that the activation energies for oxygen vacancy migration in these two systems are similar, a diffusion coefficient value of 7.2 × 10^{-15} cm^2/s was estimated at 180°C for PZT ceramics, which is very close to the diffusion coefficient measured in this work for PZT films.

Since more oxygen vacancies accumulate near the cathode upon electrical degradation in Mn-doped PZT films compared to Nb-doped samples, a higher concentration of compensating electrons is expected in Mn-doped PZT films. In principle, each oxygen vacancy is charge compensated by two electrons ($n \sim 2[V_O^{\cdot\cdot}]$), which could be trapped by the Ti^{4+} to create Ti^{3+}. Subsequent electron polaron hopping between the Ti sites in the cathodic regions was shown by Liu et al. in Fe-doped $SrTiO_3$ single crystals.[15] However, in this study, Ti^{3+} was only observed near the cathode of degraded Nb-doped PZT films. The TSDC data of Mn-doped PZT films did not show a depolarization current peak arising from a relaxation of trapped charges, though the concentration of mobile oxygen vacancies and hence the amount of compensating electronic charge is much higher compared to Nb-doped samples.

To obtain additional evidence for changes in Ti valence in the cathodic region, Nb- and Mn-doped PZT samples were investigated using EELS. Figure 9 shows a series of Ti-L edges from different positions in the PZT film as a function of distance from the Pt bottom interface (cathode). A gradual shift to lower energy loss value was observed for the Ti $L_{2,3}$ edge of Nb-doped PZT films. Moreover, Ti $L_{2,3}$ data taken close to the cathode show that the t_{2g} and e_g peaks develop noticeable shoulders (see Figure 9B). Both the chemical shift of the Ti $L_{2,3}$ to lower energy losses and the appearance of shoulders on t_{2g} and e_g imply the reduction of Ti cations.[34,35] This shows a gradual change in the Ti valence state toward the bottom electrode (cathode), suggesting more electrons near the cathodic region of Nb-doped PZT samples. In Nb-doped PZT films, long-range migration and a subsequent pile of oxygen vacancies are believed to be responsible for electrical degradation. This leads to an increase in the concentration

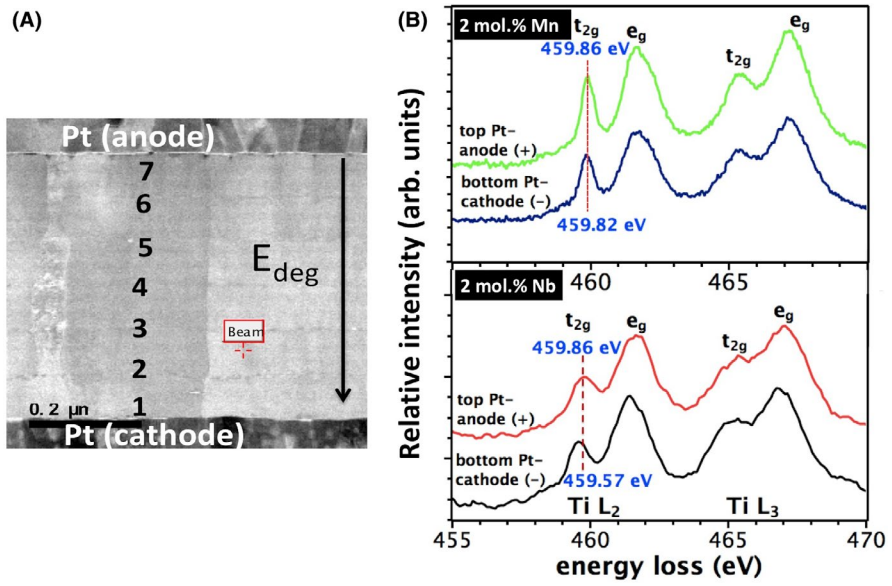

FIGURE 9 (A) Cross-sectional image of 2% Nb-doped PZT films (B) Electron energy loss spectrum from regions near the PZT /top Pt (anode) and PZT/bottom Pt (cathode) interfaces. Ti $L_{2,3}$ of Mn, and Nb-doped PZT films after degrading at 180°C under the electric field of 350 kV/cm for 12 h [Color figure can be viewed at wileyonlinelibrary.com]

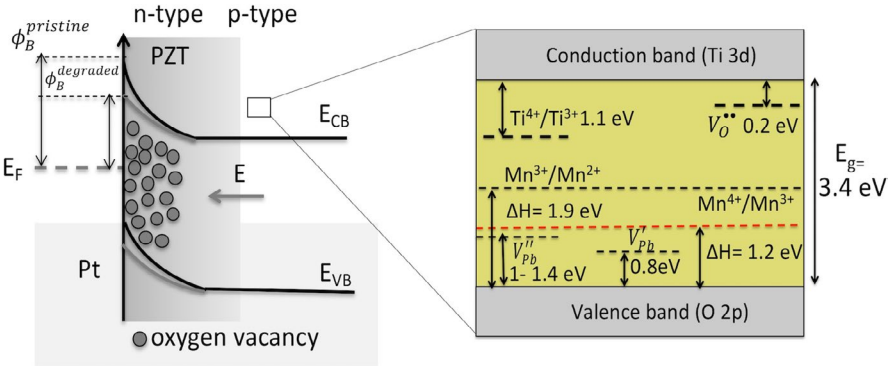

FIGURE 10 Schematic representation of energy band diagram of PZT in contact with Pt electrode. The dark and gray lines for the bands show the potential barrier height in a pristine and degraded state, respectively. Dark circles represent oxygen vacancies accumulated near the cathodic region upon electrical degradation [Color figure can be viewed at wileyonlinelibrary.com]

of compensating electrons near the cathodic region and reduction of Ti^{4+} to Ti^{3+}.[36]

For Mn-doped PZT, on the other hand, no apparent chemical shift is observed from a series of EELS spectra taken across the thickness of degraded samples, implying that there is no modification to the Ti valence in the degraded films. This suggests that although the acceptor ions increase the oxygen vacancy concentration in PZT films, free-electron generation due to compensation of oxygen vacancies at the cathode and free hole formation at the anode region might be suppressed by the valence changes from $Mn^{3+/4+}$ to $Mn^{2+/3+}$ and $Mn^{2+/3+}$ to $Mn^{3+/4+}$, respectively. Mn can take multiple valence states and the ionization energy for 2+/3+ and 3+/4+ transitions are 1.2 and 1.9 eV, [37] respectively. A schematic of the fully conceptualized model, including Ti and Mn trap states, accumulation of oxygen vacancies and band bending at the electrode interface is shown in Figure 10.38 The presence of Mn in both the 2+ and 3+ valence states in the PZT films was demonstrated in another study using deep level transient spectroscopy (DLTS).[39] Since the Mn_{Ti}^{x} and Mn_{Ti}' ions are more reducible than Ti_{Ti}', the electrons accumulated near the cathode region are trapped by Mn sites rather than Ti^{4+} ions. Due to the lower

$$Mn_{Ti}' + e' \rightleftarrows Mn_{Ti}'' \; Mn_{Ti}^{x} + e' \rightleftarrows Mn_{Ti}' \tag{11}$$

$$Mn_{Ti}'' + h^{\cdot} \rightleftarrows Mn_{Ti}' \; Mn_{Ti}' + h^{\cdot} \rightleftarrows Mn_{Ti}^{x} \tag{12}$$

concentration of Mn with respect to Ti in PZT films, trapped electrons via Mn ions are distributed over a longer length scale. This diminishes the maximum electric field at the Schottky interface, which suppresses the potential barrier height lowering and subsequent leakage current rise upon degradation. This leads to a longer lifetime and lower electrical degradation rate in Mn-doped PZT films.

5 | CONCLUSIONS

It was demonstrated that TSDC is a useful technique to understand the type of defects leading to to DC resistance degradation in PZT films. Only one relaxation current peak near 200°C was observed for Mn-doped PZT samples; this is associated with space charge polarization. Three distinct methods: the initial rise model, heating rate, and FWHM methods all gave activation energy of the TSDC peak in the range

of 0.6–0.8 eV. This peak was attributed to the migration of oxygen vacancies. The magnitude of the depolarization current peak increases with increasing Mn concentration. A similar but smaller TSDC peak attributed to the relaxation of oxygen vacancies was also observed in Nb-doped PZT films. An additional TSDC peak, associated with trapped charges, in the temperature range of 250°C–300°C, was observed in Nb-doped PZT films. The trap depth is estimated to be 0.18 ± 0.05 eV, which is attributed to electron hopping between B site ions Ti'_{Ti} and Ti^{X}_{Ti}. EELS results confirm the chemical shift in Ti $L_{2,3}$ to lower energy losses and appearance of shoulders on the t_{2g} and e_g peaks, implying reduction of Ti cations; this was observed only in degraded Nb-doped samples. It is believed that free-electron generation from the compensation of oxygen vacancies at the cathode and free hole formation at the anode region might be suppressed by the valence changes from Mn^{3+} to Mn^{2+} and Mn^{4+} to Mn^{3+} in Mn-doped films. This occurs preferentially to the reduction in Ti in Mn-doped PZT films, consistent with the location of the energy levels in the band structure.

ACKNOWLEDGMENT

The authors gratefully acknowledge financial support from the National Science Foundation, as part of the Center for Dielectrics and Piezoelectrics under Grant Nos. IIP-1841453 and IIP-1841466.

ORCID

Betul Akkopru-Akgun https://orcid.org/0000-0003-3214-9603
Daniel M. Marincel https://orcid.org/0000-0003-1487-9266
Clive A. Randall https://orcid.org/0000-0002-5478-2699
Susan Trolier-McKinstry https://orcid.org/0000-0002-7267-9281

REFERENCES

1. Wilke RH, Johnson-Wilke RL, Cotroneo V, Davis WN, Reid PB, Schwartz DA, et al. Sputter deposition of PZT piezoelectric films on thin glass substrates for adjustable x-ray optics. Appl Opt. 2013;52:3412–9.
2. Funakubo H, Dekkers M, Sambri A, Gariglio S, Shklyarevskiy I, Rijnders G. Epitaxial PZT films for MEMS printing applications. MRS Bull. 2002;37:1030–8.
3. Qiu Y, Gigliotti JV, Wallace M, Griggio F, Demore CME, Cochran S, et al. Piezoelectric Micromachined Ultrasound Transducer (PMUT) arrays for integrated sensing, actuation and imaging. Sensors. 2015;15:8020–41.
4. Benoit RR, Rudy RQ, Pulskamp JS, Polcawich RG, Bedair SS. Advances in piezoelectric PZT-based RF MEMS components and systems. J. Micromech Microeng. 2017;27(8):083002.
5. Yeo HG, Ma X, Rahn C, Trolier-McKinstry S. Efficient piezoelectric energy harvesters utilizing (001) textured bimorph PZT films on flexible metal foils. Adv Funct Mater. 2016;26(32):5940–6.
6. Yoon S-H, Randall CA, Hur K-H. Difference between resistance degradation of fixed valence acceptor (Mg) and variable valence acceptor (Mn)-doped $BaTiO_3$ ceramics. J Appl Phys. 2010;108:064101.
7. Stolichnov I, Tagantsev A, Setter N, Okhonin S, Fazan P, Cross JS, et al. Constant-current study of dielectric breakdown of Pb(Zr, Ti)$_O$3 ferroelectric film capacitors. Integrated Ferroelectr. 2001;32:45.
8. Zhang SJ, Liu W, Donnelly NJ, Xu Z, Randall CA. Time dependent dc resistance degradation in lead-based perovskites: 0.7 $Pb(Mg_{1/3}Nb_{2/3})O_3$–0.3$PbTiO_3$. J Appl Phys. 2009;105:053705.
9. Zafar S, Hradsky B, Gentile D, Chu P, Jones RE, Gillespie S. Resistance degradation in barium strontium titanate thin films. J Appl Phys. 1999;86:06410.
10. Wang R-V, McIntyre PC. ^{18}O tracer diffusion in $PbZrTiO_3$ thin films: a probe of local oxygen vacancy concentration. J Appl Phys. 2005;97:023508.
11. Prisedsky V, Shishkovsky VI, Klimov VV. High-temperature electrical conductivity and point defects in lead zirconate-titanate. Ferroelectrics. 1978;17:465.
12. Waser R, Baiatu T, Härdtl KH. dc electrical degradation of perovskite-type titanates: I, ceramics. J Am Ceram Soc. 1990;73:1654.
13. Smyth DM. Ionic transport in ferroelectrics. Ferroelectrics. 1994;151:115.
14. Raymond MV, Smyth DM. Defects and charge transport in perovskite ferroelectrics. J Phys Chem Solids. 1996;57:1507.
15. Liu W, Randall CA. Thermally stimulated relaxation in Fe-doped $SrTiO_3$ systems: I. single crystals. J Am Ceram Soc. 2008;91(3245).
16. Liu W, Randall CA. Thermally stimulated relaxation in Fe-doped $SrTiO_3$ systems: II. degradation of $SrTiO_3$ dielectrics. J Am Ceram Soc. 2008;91:3251.
17. Takeoka S, Morita K, Mizuno Y, Kishi H. Thermally stimulated current (TSC) studies on resistance degradation of Ni-MLCC. Ferroelectrics. 2007;356:370.
18. Wu Z, Sayer M. Defect structure and fatigue in ferroelectric PZT thin films. Applications of ferroelectrics. Proc Eighth IEEE Int Symp. 1992;244.
19. Okino H, Shimizu M, Horiuchi T, Shiosaki T, Matsushige K. A study of the defect structures in MOCVD-grown $PbZr_xTi_{1-x}O_3$ thin films by thermally stimulated current measurements. Integr Ferroelectr. 1997;18:63.
20. Wolf RA, Trolier-McKinstry S. Temperature dependence of the piezoelectric response in lead zirconate titanate films. J Appl Phys. 2004;95(3):1397–406.
21. Akkopru-Akgun B, Zhu W, Lanagan MT, Trolier-McKinstry S. The effect of imprint on remanent piezoelectric properties and ferroelectric aging of Mn or Nb doped $PbZr_{0.52}Ti_{0.48}O_3$ thin films. J Am Soc. 2019;102(9):5328–41.
22. Marincel DM, Belianinov SJA, Okatan MB, Kalinin SV, Jackson TN, Randall CA, et al. A-site stoichiometry and piezoelectric response in thin film $PbZr_{1-x}Ti_xO_3$. J Appl Phys. 2015;117:204104.
23. Akkopru-Akgun B, Zhu W, Randall CA, Lanagan MT, Trolier-McKinstry S. Polarity dependent DC resistance degradation and electrical breakdown in Nb doped PZT films. APL Mater. 2019;7(12):120901.
24. Chen R, Kirsh Y. Analysis of thermally stimulated process. New York, NY: Pergamon Press; 1981. p. 146.
25. Torres A, Jimenez J, Vega B, De Saja JA. Influence of heating rate in the dipolar relaxation. Phys Stat Sol (A). 1985;90:749.

26. Braunlich P. Thermally stimulated relaxation in solids. New York, NY: Springer; 1979. p. 75–160.
27. Jonscher AK. Dielectric relaxation in solids. London: Chelsea Dielectrics Press; 1983. p. 233–50.
28. Liu W-E. Impedance/thermally stimulated depolarization current and microstructural relations at interfaces in degraded perovskite dielectrics. PhD thesis. Penn State University. 2009;28–34.
29. Chen R, Kirsh Y. Analysis of thermally stimulated processes. New York, NY: Pergamon Press; 1981. p. 65–82.
30. Moura Ramos JJ, Correia NT. The determination of the activation energy of a relaxational process from thermally stimulated depolarisation currents (TSDC) data: an illustration with the β-relaxation of maltitol. Thermochim Acta. 2005;426:185.
31. Chen J, Harmer MP, Smyth DM. Compositional control of ferroelectric fatigue in perovskite ferroelectric ceramics and thin films. J Appl Phys. 1994;76:5394.
32. Zhao S, Zhang SJ, Liu W, Donnelly NJ, Xu Z, Randall CA. Time dependent dc resistance degradation in lead-based perovskites $0.7Pb(Mg_{1/3}Nb_{2/3})O_3$–$0.3PbTiO_3$. J Appl Phys. 2009;105:053705.
33. Van Turnhout J. Thermally stimulated discharge of polymer electrets. Amsterdam: Elsevier. 1975;161.
34. Leapman RD, Grunes LA, Fejes PL. Study of the L_{23} edges in the 3d transition metals and their oxides by electron-energy-loss spectroscopy with comparisons to theory. Phys Rev B. 1982;26:614.
35. Otten MT, Miner B, Rask JH, Buseck PR. The determination of Ti, Mn and Fe oxidation states in minerals by electron energy-loss spectroscopy. Ultramicroscopy. 1985;18:285.
36. Akkopru-Akgun B, Bayer T, Tsuji K, Randall CA, Lanagan MT, Trolier-McKinstry S. Leakage current characteristics and DC resistance degradation mechanisms in Nb doped PZT films. J Appl Phys. 2021;29:174102,1–12.
37. Wechsler BA, Klein MB. Thermodynamic point defect model of barium titanate and application to the photorefractive effect. J Opt Soc Am B- Opt Phys. 1988;5:1711–23.
38. Akkopru-Akgun B. The role of defect chemistry in DC resistance degradation of lead zirconate titanate thin films. PhD thesis. Penn State University. 2019;2–6.
39. Akkopru-Akgun B, Bayer JM, Tsuji K, Randall CA, Lanagan MT, Trolier-McKinstry S. The influence of Mn doping on the leakage current mechanisms and resistance degradation behavior in lead zirconate titanate thin films. Acta Mater. 2021;208:116680, 1–8.
40. Härdtl KH, Rau H. PbO vapour pressure in the $Pb(Ti_{1-X})O_3$ system. Solid State Commun. 1969;7:41.

How to cite this article: Akkopru-Akgun B, Marincel DM, Tsuji K, et al. Thermally stimulated depolarization current measurements on degraded lead zirconate titanate films. *J Am Ceram Soc*. 2021;104: 5270–5280. https://doi.org/10.1111/jace.17891